NANO LETTERS

Letter

pubs.acs.org/NanoLett

Nanoscale Transport Enables Active Self-Assembly of Millimeter-Scale Wires

Ofer Idan, Amy Lam, Jovan Kamcev, John Gonzales, Ashutosh Agarwal, and Henry Hess*

Department of Biomedical Engineering, Columbia University, New York, New York, United States

Supporting Information

ABSTRACT: Active self-assembly processes exploit an energy source to accelerate the movement of building blocks and intermediate structures and modify their interactions. A model system is the assembly of biotinylated microtubules partially coated with streptavidin into linear bundles as they glide on a surface coated with kinesin motor proteins. By tuning the assembly conditions, microtubule bundles with near millimeter length are created, demonstrating that active self-assembly is beneficial if components are too large for diffusive self-assembly but too small for robotic assembly.

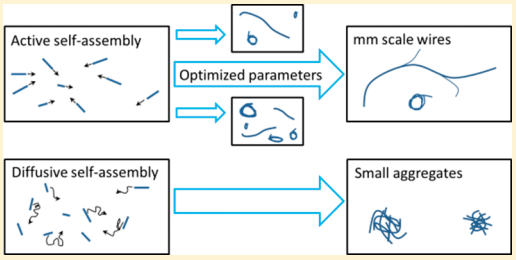

KEYWORDS: *Self-assembly, active transport, biomolecular motor, nanowire, kinesin, microtubule*

The integration of molecular and nanoscale components into functional macroscopic systems is one of the central challenges in nanotechnology. On the bottom-up route, the challenge arises from the unfavorable scaling of diffusion-driven self-assembly with increasing component size.[1,2] On the top-down route, the sequential nature of robotic assembly is ill-suited to the high throughput required by the large number of microscopic components.[3] Natural growth processes, e.g., embryogenesis, assemble complex macroscopic structures by using motile cells which position themselves using active, energy-consuming movement.[4] Endowing molecular and nanoscale building blocks with the ability to autonomously move, e.g., by loading them onto molecular shuttles, may similarly overcome the limitations of diffusion-driven self-assembly.

Here it is shown experimentally that active transport by biomolecular motors can assemble structures of nearly 1 mm in length from building blocks only about 10 μm in size. A basic theoretical model of the assembly process illustrates the advantages and limitations of active transport processes relative to diffusion-driven self-assembly and robotic assembly.

The experimental model system is the assembly of extended bundles of biotinylated microtubules cross-linked by streptavidin via active transport on a kinesin-coated surface (Figure 1). Microtubules are cytoskeletal filaments with a diameter of 25 nm assembled from thousands of tubulin subunits.[5] When polymerized in vitro, their lengths are described by a Schulz distribution with an average length on the order of 5 μm.[6] Kinesin motor proteins adhered to a surface can transport microtubules with a velocity of hundreds of nanometers per second[7,8] on a trajectory which can be described by a worm-like chain model with a persistence length of 0.1 mm.[9] Biotinylated microtubules can be cross-linked with streptavidin. When cross-linking occurs during microtubule gliding on kinesin-coated surfaces, extended linear bundles and spools of microtubules are formed.[10,11] This process is a striking example of an active self-assembly process[12] and has been investigated in several recent studies.[13−20] Here we show that by optimizing the microtubule transport velocity, which affects the time available for biotin−streptavidin binding[21] and reduces spool formation,[18] microtubule bundles with near millimeter lengths can be formed. This represents a 10-fold increase in the reported size of the assembled microtubule structures.[22]

In our experiments, biotinylated microtubules were adsorbed to kinesin-coated surfaces and exposed to a 10 nM streptavidin solution for 5 min. This leads to partial coverage of the biotin linkers on the microtubules, enabling cross-linking when microtubules collide. Varying the microtubule gliding velocity by adjusting kinesin motor activity via the ATP concentration in the solution affected the length of the longest observed microtubule bundles. The ATP concentration was maintained at a constant level for hours by employing an ATP regenerating system.[23] Otherwise, the assembly process is arrested at low ATP concentrations by a lack of ATP within an hour. ATP concentrations of 20 μM (corresponding to gliding speeds of 0.1 μm/s) proved optimal (Supporting Information, Figure S1). Collisions of the gliding microtubules lead to the formation of bundles, which collide with each other and form even larger linear bundles. Bundles are converted into spools when simultaneous collisions of multiple bundles create circular topologies or when the tip of the bundle encounters a defective motor and its movement is arrested leading to a spiraling movement and the formation of a spool.[17] Therefore, bundles are transient structures (unless gliding is stopped by removal of ATP or chemical fixation) and require a suitable combination of initial microtubule densities, streptavidin concentrations,

Received: October 3, 2011
Revised: November 21, 2011
Published: November 24, 2011

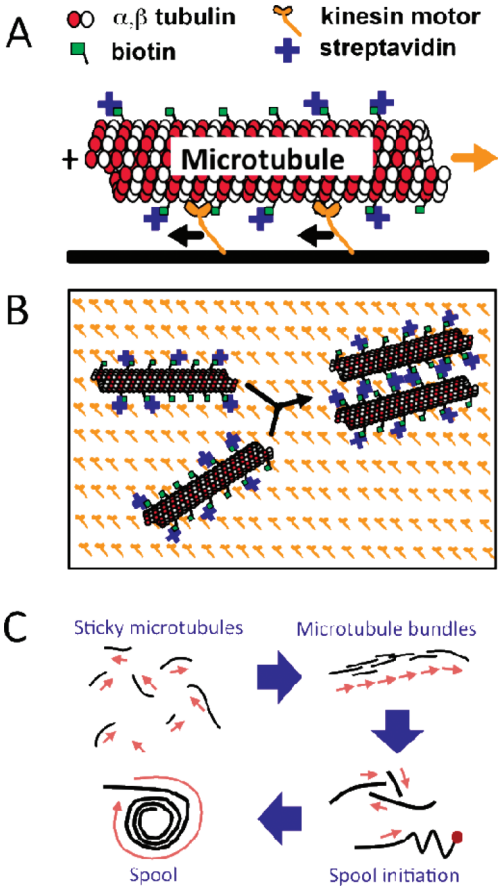

Figure 1. (A) Surface-adhered kinesin motor proteins can transport biotinylated microtubules with gliding velocities up to 1 μm/s. (B) A partial coating with streptavidin enables microtubules to cross-link into microtubule bundles. (C) Individual microtubules and microtubule bundles can form "spools" either when three or more microtubules simultaneously collide or when a defective motor arrests the gliding of a microtubule tip.

degrees of microtubule biotinylation, ATP concentration, and assembly time.

The largest observed microtubule bundle, identified by manually surveying the flow cell, reached nearly 1 mm in length and was imaged 2 h after the microtubule movement was initiated (Figure 2A). Bundles of more than half a millimeter in length were repeatedly observed (Supporting Information, Figure S2). Since the bundles covered multiple fields-of-view, overlapping images were stitched together using NIH Image software.

The microtubule bundle in Figure 2A consists of 4000 microtubules, based on a comparison of the bundle brightness to the brightness of individual microtubules (Supporting Information). These 4000 microtubules were recruited from microtubules covering the surface initially at a density of 6000 mm^{-2}.

In contrast, no such structures were found in experiments in which diffusion was the primary mode of microtubule transport. In these experiments, 3 μL of a solution containing biotinylated microtubules and 3, 5, or 10 nM of streptavidin were placed between two casein-coated coverslips and sealed against evaporation. Due to the casein coating, the microtubules did not attach onto the surface of the glass slide and were able to diffuse freely. Again, collisions of these diffusing microtubules led to the formation of larger aggregates due to

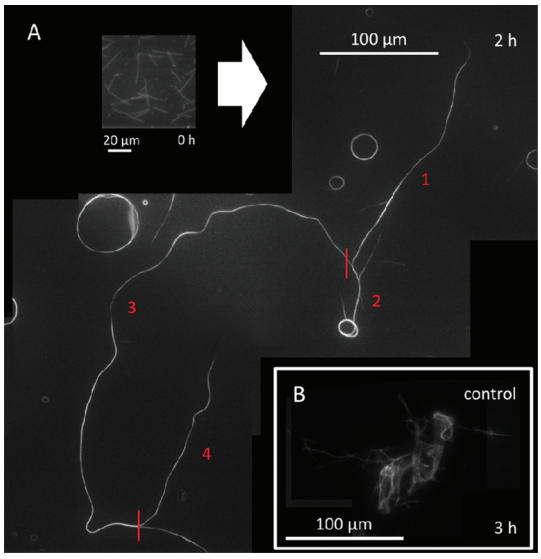

Figure 2. Experimental results. (A) Active transport by kinesin motors assembles individual microtubules into linear bundles and spools. The longest structure reached a size of almost 1 mm (segments 1–4: 222, 49, 503, 166 μm, respectively). (B) The largest microtubule aggregate observed when microtubules assemble only via two-dimensional diffusion in a chamber of 3 μm height.

the cross-linking of streptavidin and biotin. However, without the directed and forceful movement imparted by the kinesin motors acting on the microtubules, these aggregates were disordered and had no discernible structure. The largest aggregates observed were only 0.1 mm in diameter (Figure 2B).

The advantages and limitations of an active self-assembly process over diffusion-driven self-assembly can be illustrated by a simple theoretical model. Inspired by Kuhn and Försterling's derivation of the diffusion-limited reaction rate,[24] we model the assembling microtubules and bundles as spherical particles with a radius proportional to the microtubule/bundle length moving on a two-dimensional surface (Figure 3). All particles are assumed to have a uniform size which increases with time as a result of the assembly process. The surface is conceptually divided into sites of equal size, which are either occupied by the particles or empty. Particles hop between sites at a rate determined by their radius and the transport mode (diffusive with diffusion constant D or active with velocity v). According to our understanding of the experimental system,[17] the assembly process is approximated by three events: (A) Two particles meet and fuse into one larger particle which continues to participate in the assembly process; (B) three particles simultaneously meet and form a spool; and (C) a particle spontaneously converts into a spool as a result of pinning of the leading tip of the gliding microtubule bundle. The spools formed by processes (B) and (C) are discounted from the further assembly process.

Alternative modeling approaches can be found in the literature of aggregation and fragmentation processes.[25,26] Existing models of self-assembly processes, such as the tile assembly model, assume very simplified transport processes where depletion of building blocks or slowing of movement with increasing size is not considered.[27−31] The focus of the model presented here is the impact of the scaling of the transport processes on the assembly kinetics, while the complexities introduced by specific interactions or constraints on building block paths and orientations are entirely

dx.doi.org/10.1021/nl203450h | Nano Lett. 2012, 12, 240−245

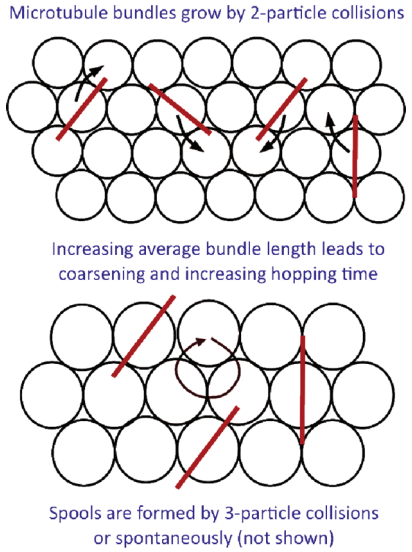

Figure 3. Basic model of the assembly process considers microtubules and microtubule bundles (straight lines) as particles with a uniform size (given by the average size of the microtubules and bundles in the experiment) and an orientation-averaged interaction radius. Particles hop to new surface sites with a time constant given by the transport mode (diffusive or active). Collisions between two particles reduce the number of particles, increase the average size, and consequently change the interaction radius and hopping time. Spools are formed by three-particle collisions or spontaneously (mimicking the encounter with defective motors).

neglected.[32] The presented model is a "hopping" model which can model both diffusive[33] and active[34] transport.

Focusing first on process (A), the growth of microtubule bundles, in the absence of the spool-forming processes (B) and (C), we can write for the number N of microtubules and microtubule bundles on a surface with area A:

$$\frac{dN}{dt} = -\frac{1}{\tau} \times N \times 6\pi R^2 \frac{N}{A} \tag{1}$$

reflecting the probability that at a given time step, one of the six neighboring sites of a particle will be filled by another particle multiplied by the number of particles with τ as hopping time and R as the interaction radius.

The hopping time τ increases with the interaction radius according to

$$\tau = \frac{(2R)^2}{4D} = \frac{R^2}{D} \tag{2a}$$

for diffusive transport, and

$$\tau = \frac{2R}{v} \tag{2b}$$

for active transport.

The interaction radius R is a fraction f of the length L of a microtubule bundle, because two microtubules/bundles can interact with each other over distances which are dependent on their relative orientation. Furthermore, the average length of a microtubule bundle increases as the number of microtubules/bundles falls from its initial value N_0 due to bundling. The approximate increase in length is (see Supporting Information):

$$R = fL = fL_0\sqrt{\frac{N_0}{N}} \tag{3}$$

This relationship approximates the increase in length resulting from the incorporation of a colliding microtubule/bundle into an existing microtubule/bundle at a random location along the existing microtubule/bundle. It also holds more generally for aggregation in two dimensions.

Furthermore, the diffusion coefficient of the microtubules/bundles is size dependent according to[35]

$$D = \frac{6kT}{3\pi\eta L} \tag{4}$$

Solving eq 1, using eqs (2a–4) and inserting the solution into eq 3, yields an equation for the growth of the microtubules/bundles:

$$L = L_0 \times \left(1 + \frac{18kT\sigma_0 t}{\eta L_0}\right)^{1/3} \tag{5a}$$

for diffusive transport, and

$$L = L_0\left(1 + \frac{3}{2\pi} f L_0 \sigma_0 v t\right) \tag{5b}$$

for active transport, where L_0 is the initial length of the microtubules, kT = 4 pNnm is the thermal energy at room temperature, σ_0 is the initial microtubule density, $\eta = 10^{-3}$ Pas is the viscosity of water, v is the velocity of the microtubules gliding on kinesin, and $f = 4/\pi^2$ is the ratio of effective radius to microtubule length.

For the experiment shown in Figure 2, the initial average length was determined to be 12 μm (118 microtubules measured in 3 fields of view), and the initial microtubule density was measured to be of 6000 mm^{-2}. The gliding velocity under our experimental conditions (0.02 mM ATP, 18 °C) is 0.1 μm/s.[8] Under these conditions, the assembly speed (the derivative of the time-dependent length) of active transport equals 0.7 μm/s and exceeds the assembly speed of diffusive transport (0.3 μm/s at t = 0 s) at all times. However, for smaller building blocks or smaller active transport velocities, diffusive transport has an initial advantage, as one would expect.

According to eqs 5a and 5b, the transition from diffusive to active transport is already beneficial at the very beginning of the assembly process if the initial length of the building blocks L_0 exceeds

$$L_{\text{threshold}} = \sqrt{\frac{\pi kT}{\eta v}} \tag{6}$$

For our assembly conditions (room temperature, viscosity of water, and microtubule gliding velocity of 0.1 μm/s), this threshold length is equal to 10 μm. If the size of the building blocks is substantially below this threshold length, a hierarchical assembly process with distinct stages of diffusive transport and active transport is desirable. For example, microtubules are assembled from tubulin proteins by diffusion-based transport, while the assembly of mitotic spindles and our microtubule bundles relies on active transport.[12]

If processes (B) and (C), the formation of spools by the simultaneous collisions of three microtubules/bundles and the formation of spools as a result of tip pinning by defective motors, are included in the modeling, eq 1 is modified by

dx.doi.org/10.1021/nl203450h | Nano Lett. 2012, 12, 240–245

additional terms:

$$\frac{dN}{dt} = -\frac{dN_{bundle}}{dt} - 3\frac{dN_{spool}^{three}}{dt} - \frac{dN_{spool}^{pinning}}{dt} \quad (7)$$

These additions lead to coupled differential equations for the surface density of microtubules/bundles and their length (for details see Supporting Information):

$$\frac{d\sigma}{dt} = -12\frac{kT}{\eta}\left(\frac{\sigma^2}{L} + \frac{32}{\pi^3}L\sigma^3\right) \quad (8a)$$

$$\frac{dL}{dt} = \frac{6kT}{\eta}\sigma \quad (9a)$$

for diffusive transport (where defective motors are absent), and

$$\frac{d\sigma}{dt} = -\frac{12}{\pi}vL\sigma^2 - \frac{384}{\pi^4}vL^3\sigma^3 - \frac{v\sigma}{d_{defective}} \quad (8b)$$

$$\frac{dL}{dt} = \frac{6}{\pi}vL^2\sigma \quad (9b)$$

for active transport. Here, eq 3 does not apply, because spools remove microtubules and bundles from the pool. The numerical solution of these equations for $\eta = 10^{-3}$ Pas, $v = 0.1$ μm/s, $d_{defective} = 1$ mm (according to Nitta et al.[9]), L(0) = 12 μm,and $\sigma(0) = 6000$ mm^{-2} is shown in Figure 4.

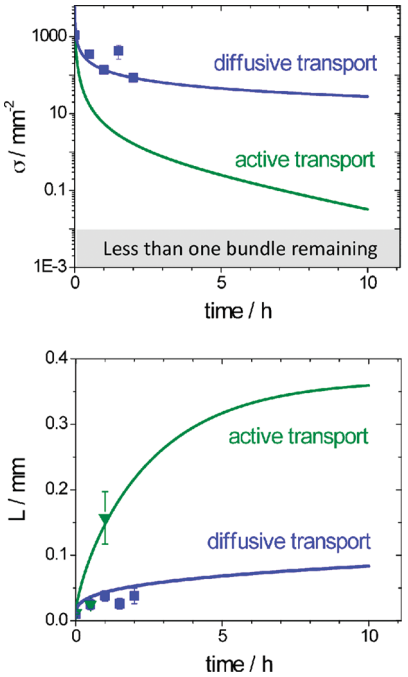

Figure 4. In the assembly model (solid lines), the microtubule/bundle density drops exponentially as a result of bundling and spool formation processes. At the same time, the length of the bundles increases to several hundred micrometers if the microtubules/bundles move as a result of active transport. In contrast, diffusive transport leads to slower growth of bundles, due to the lower frequency of collisions. The limited size of the cell in which assembly happens (~1 cm^2) defines a lower limit for the density (~10^{-2} mm^{-2}). The acquisition of experimental data, in particular of the density of microtubules and bundles for active transport, is hampered by the small field-of-view of the microscope (see Supporting Information).

From the numerical analysis of the diffusive transport case (eqs 8a and 9a), one finds that at long times the rate of spool formation (σ^2/L) decreases faster than the rate of bundling events ($L\sigma^3$) due to the different scaling. At long times, the bundle density evolves in proportion to $1/t$ and the bundle length increases with the logarithm of time. Bundle growth proceeds indefinitely due to an absence of growth-arresting mechanisms in the model, such as nonspecific binding of bundles to a surface.

For the active transport case (eqs 8b and 9b), the equations show that when $\sigma \gg L^{-2}$, spooling via three particle collisions dominates the dynamics and leads to a rapid drop in particle density. The microtubules/bundles contributing to spool formation are removed from the system without extending bundles. As a result, increasing the initial density beyond L_0^{-2} increases the final length of the microtubules/bundles only marginally. At long times, when $\sigma \ll 1/Ld_{defective}$, the kinetics is dominated by an exponential removal of microtubules/bundles from the system via spool formation due to tip pinning. Therefore, growth of bundles from collisions slows, and bundle length reaches a plateau. The position of the plateau is most sensitive to the distance between surface defects which cause tip pinning; for distances above 4 mm, the model predicts that bundles reach more than 1 mm in length. Finally, the terms on the right-hand side of eqs 8b and 9b scale linearly with velocity, so that doubling the velocity merely halves the time to reach a certain point in the assembly process. However, in the experiment the movement of the microtubules/bundles may be affected in subtle ways by changes in velocity. For example, a lower velocity gives a microtubule pinned to a surface defect more time to break free before a spool has formed.

The acceleration of the assembly process by active transport is caused by both an increase in the average velocity of the building blocks and the sustained movement in one direction. Since the path of microtubules/bundles is affected by thermal fluctuations, the direction of movement is randomized over time.[36] This process can be described by a trajectory persistence length, which for the kinesin/microtubule system is equal to 0.1 mm.[9,37,38] Because the microtubule path is determined by the behavior of the leading tip,[39] microtubule bundles which are terminated by individual microtubules should have an identical trajectory persistence length. As travel distances approach the trajectory persistence length, the character of the active transport changes from a ballistic to a diffusive regime.[40] In the diffusive regime, the microtubule/bundle trajectory can be described by a diffusion coefficient $D = vL_p$, where v is the gliding velocity and L_p is the trajectory persistence length. For the kinesin/microtubule system ($v = 0.1$ μm/s, $L_p = 0.1$ mm), this "gliding" diffusion coefficient is similar to the "free" diffusion coefficient of a 4 μm long microtubule (Supporting Information, eq 4). So for small bundles (<100 μm), the accelerated assembly stems from the ballistic trajectories at this length scale. For large bundles (>100 μm), the active movement loses its directedness, but the "gliding" diffusion coefficient does not diminish with size in contrast to the "free" diffusion coefficient. Our simple analytical model does not capture this transition and thus somewhat overestimates the benefit of active transport. Since the model calculates an average bundle size, while our experiments have focused on finding the largest aggregates due to the difficulty of imaging an entire flow cell (~2500 fields of view), the larger size of the observed structures (Figure 2) relative to the model predictions (Figure 4) should be expected.

dx.doi.org/10.1021/nl203450h | Nano Lett. 2012, 12, 240–245

A hierarchy of assembly processes emerges from the above considerations. Self-assembly based on diffusive transport is the preferred assembly process at the nano- to microscale. Self-assembly relying on active transport can accelerate assembly processes at the microscale. Robotic assembly wins at the millimeter scale, particularly when only a small number of structures has to be fabricated.[3]

Of course, a variety of alternative approaches can be utilized to accelerate the diffusive self-assembly of microparticles. For example, a high concentration of building blocks at the assembly site can be maintained by sedimentation or evaporation of the solvent.[41,42] The relative merit of these alternatives has to be evaluated on a case-by-case basis. Solvent evaporation, for example, is energetically costly relative to active transport by highly efficient biomolecular motors.

Similarly, the active self-assembly process can be enhanced if the building blocks are attracted to each other or a specific assembly site. Self-propelled nanorods, for example, can exhibit chemotactic behavior.[43] Biological cells self-assemble by responding to chemical and mechanical cues with active and directed movement. However, the creation of steep chemical gradients at the microscale is energetically costly as well.[44]

In summary, we have experimentally shown that microtubule bundles nearly a millimeter in length can be formed by active self-assembly. This demonstrates the promise of active transport by molecular motors for mesoscale assembly, bridging the gap between self-assembly relying on diffusion and robotic assembly. Our basic models indicate that, while diffusive self-assembly is faster initially, active self-assembly becomes faster roughly when the product of building block size and active transport velocity exceeds the diffusion coefficient of the building blocks. Furthermore, in the case of microtubule bundle assembly, bundle length is limited to about 1 mm by the processes leading to spool formation. The utility of molecular motors and nanoscale transporters in active self-assembly provides a justification for further efforts to develop hybrid and synthetic systems.[45]

Materials and Methods. The "active transport" experiments were performed at a temperature of 18 °C in approximately 100 μm high and 1 cm wide flow cells assembled from two coverslips and double-stick tape.[46] A kinesin construct consisting of the wild-type, full-length *Drosophila melanogaster* kinesin heavy chain and a C-terminal His-tag was expressed in *Escherichia coli* and purified using a Ni-NTA column.[47] Microtubules were prepared by polymerizing 20 μg of biotin-labeled tubulin (Cytoskeleton Inc., Denver, CO) in 6.5 μL of growth solution containing 4 mM of $MgCl_2$, 1 mM of GTP, and 5% DMSO (v/v) in BRB80 buffer for 30 min at 37 °C. The microtubules were then 100-fold diluted and stabilized in 10 μM paclitaxel (Sigma, Saint Louis MO).

The flow cells were first filled with a solution of casein (0.5 mg/mL, Sigma) dissolved in BRB80 (80 mM of PIPES, 1 mM of $MgCl_2$, 1 mM of EGTA, and pH of 6.9). After 5 min, it was exchanged with a kinesin solution (10 nM in BRB80 with 0.5 mg/mL of casein and 0.02 mM of ATP). After another 5 min, this was exchanged against a motility solution (10 μM of paclitaxel, an antifade system made up of 20 mM of D-glucose, 20 μg/mL of glucose oxidase, 8 μg/mL of catalase, 10 mM of dithiothreitol, and 0.02 mM of ATP in BRB80) containing varying concentrations of biotinylated microtubules (0.6, 0.9, 1.2, and 1.5 μg/mL) and was injected for 5 min followed by two washes of motility solution (without biotinylated microtubules) to remove excess biotin. Then 20 μL of an 80 nM solution of Alexa568-labeled streptavidin solution (Invitrogen Inc.) in BRB80 with 0.5 mg/mL of casein and 10 μM of paclitaxel was injected, followed by two washes with 20 μL of motility solution.

Each flow cell was immediately moved to an epi-fluorescence microscope (Nikon TE2000), and images of 4 different fields of view were taken using a 100× oil objective. The flow cell was imaged again 30, 60, 120, and 180 min after the last wash with antifade solution.

The "diffusion" experiments were performed at 23 °C. Microtubules were prepared as described above and diluted 500-fold (BRB80 with 0.025 mg/mL of casein and 10 μM of paclitaxel) to match the microtubule surface density of the "active transport" experiments. On top of a casein-coated glass coverslip, 1.5 μL of the microtubule solution was placed, followed by the addition of 1.5 μL of fluorescently labeled streptavidin (Alexa Fluor 488, Invitrogen). The concentration of streptavidin was varied (3, 5, and 10 nM) to match the streptavidin coverage on the microtubules in the "active transport" experiments. Immediately after the streptavidin was added, another casein-coated glass coverslip was placed on top of the 3 μL drop, and the solution spread out over the surface of the glass coverslip resulting in a chamber approximately 3 μm high. The edges of the top coverslip were lined and sealed with grease. Images of 4 different fields of view were taken using a 100× oil objective at 0, 30, 60, and 120 min after the chamber was sealed.

■ ASSOCIATED CONTENT

Ⓢ Supporting Information

Additional images of long wires obtained under various experimental conditions, details of the control experiments using diffusive transport, analytical derivation of the assembly model, and analysis of the obtained long wire images including length and density measurements and number of microtubules in the longest wire found. This material is available free of charge via the Internet at http://pubs.acs.org.

■ AUTHOR INFORMATION

Corresponding Author

*E-mail: hh2374@columbia.edu. Telephone: (212) 854-7749.

■ ACKNOWLEDGMENTS

Financial support through NSF grant DMR0645023 is gratefully acknowledged.

■ REFERENCES

(1) Service, R. F. *Science* **2005**, *309* (5731), 95−95.
(2) Mann, S.; Colfen, H. *Angew. Chem., Int. Ed.* **2003**, *42* (21), 2350−2365.
(3) Morris, C. J.; Stauth, S. A.; Parviz, B. A. *IEEE Trans. Adv. Packag.* **2005**, *28* (4), 600−611.
(4) Steinberg, M. S. *J. Exp. Zool.* **1970**, *173* (4), 395−434.
(5) Howard, J. *Mechanics of Motor Proteins and the Cytoskeleton*; Sinauer: Sunderland, MA, 2001; p 367.
(6) Jeune-Smith, Y.; Hess, H. *Soft Matter* **2010**, *6*, 1778−1784.
(7) Vale, R. D.; Reese, T. S.; Sheetz, M. P. *Cell* **1985**, *42* (1), 39−50.
(8) Tucker, R.; Saha, A. K.; Katira, P.; Bachand, M.; Bachand, G. D.; Hess, H. *Small* **2009**, *5* (11), 1279−1282.
(9) Nitta, T.; Hess, H. *Nano Lett.* **2005**, *5* (7), 1337−1342.
(10) Hess, H.; Clemmens, J.; Brunner, C.; Doot, R.; Luna, S.; Ernst, K.-H.; Vogel, V. *Nano Lett.* **2005**, *5* (4), 629−633.
(11) Bachand, M.; Trent, A. M.; Bunker, B. C.; Bachand, G. D. *J. Nanosci. Nanotech.* **2005**, *5* (5), 718−722.

(12) Hess, H. *Soft Matter* **2006**, *2* (8), 669−677.
(13) Liu, H. Q.; Spoerke, E. D.; Bachand, M.; Koch, S. J.; Bunker, B. C.; Bachand, G. D. *Adv. Mater.* **2008**, *20* (23), 4476−4481.
(14) Kawamura, R.; Kakugo, A.; Shikinaka, K.; Osada, Y.; Gong, J. P. *Biomacromolecules* **2008**, *9* (9), 2277−2282.
(15) Kakugo, A.; Tamura, Y.; Shikinaka, K.; Yoshida, M.; Kawamura, R.; Furukawa, H.; Osada, Y.; Gong, J. P. *J. Am. Chem. Soc.* **2009**, *131* (50), 18089−18095.
(16) Kawamura, R.; Kakugo, A.; Osada, Y.; Gong, J. P. *Nanotechnology* **2010**, *21* (14), 145603.
(17) Luria, I.; Crenshaw, J.; Downs, M.; Agarwal, A.; Seshadri, S. B.; Gonzales, J.; Idan, O.; Kamcev, J.; Katira, P.; Pandey, S.; Nitta, T.; Phillpot, S. R.; Hess, H. *Soft Matter* **2011**, *7* (7), 3108−3115.
(18) Liu, H.; Bachand, G. D. *Soft Matter* **2011**, *7* (7), 3087−3091.
(19) Crenshaw, J. D.; Liang, T.; Hess, H.; Phillpot, S. R. *J. Comput. Theor. Nanosci.* **2011**, *8* (10), 1999−2005.
(20) Liu, L.; Tuzel, E.; Ross, J. L. *J. Phys: Condens. Matter* **2011**, *23*, 374104.
(21) Agarwal, A.; Katira, P.; Hess, H. *Nano Lett.* **2009**, *9* (3), 1170−1175.
(22) Kawamura, R.; Kakugo, A.; Osada, Y.; Gong, J. P. *Langmuir* **2010**, *26* (1), 533−537.
(23) Leduc, C.; Ruhnow, F.; Howard, J.; Diez, S. *Proc. Natl. Acad. Sci. U.S.A.* **2007**, *104* (26), 10847−10852.
(24) Kuhn, H.; Foersterling, H.-D. *Principles of Physical Chemistry: Understanding Molecules, Molecular Assemblies, Supramolecular Machines*; Wiley: Chichester, U.K., 1999; p 970.
(25) Wattis, J. A. D. *Phys. D* **2006**, *222* (1−2), 1−20.
(26) Bellomo, N.; Bianca, C.; Delitala, M. *Phys. Life Rev.* **2009**, *6* (3), 144−175.
(27) Rothemund, P. W. K.; Winfree, E. The Program-Size Complexity of Self-Assembled Squares. In *Proceedings of the 32nd Annual ACM Symposium on Theory of Computing (Proceedings of the Annual ACM Symposium on Theory of Computing)*, 2000; ACM: New York; pp 459−468.
(28) Adleman, L.; Cheng, Q.; Goel, A.; Huang, M. Running Time and Program Size for Self-Assembled Squares. In *Proceedings of the 33rd Annual ACM Symposium on Theory of Computing (Proceedings of the Annual ACM Symposium on Theory of Computing)*; ACM: New York, 2001; pp 740−748.
(29) Becker, F.; Rapaport, I.; Remila, E. *Foundations of Software Technology and Theoretical Computer Science*; Springer-Verlag: Berlin, Heidelberg, Germany, 2006; pp 45−56.
(30) Chen, H.; Doty, D. Parallelism and Time in Hierarchical Self-Assembly. In the *23rd Annual ACM-SIAM Symposium on Discrete Algorithms*; SIAM: Philadelphia, Pennsylvania, 2012, http://arxiv.org/abs/1104.5226.
(31) Klavins, E.; Burden, S.; Napp, N. Optimal Rules for Programmed Stochastic Self-Assembly. In *Proceedings of Robotics: Science and Systems*; MIT: Cambridge, MA, 2006; pp 9−16.
(32) Napp, N.; Burden, S.; Klavins, E. *Autom. Rob.* **2011**, *30* (1), 57−71.
(33) Berg, H. C., *Random walks in biology*. Princeton University Press: Princeton, N.J., 1983; Vol. *ix*, p 142.
(34) Chowdhury, D.; Santen, L.; Schadschneider, A. *Phys. Rep.* **2000**, *329* (4−6), 199−329.
(35) Tirado, M. M.; Martinez, C. L.; Delatorre, J. G. *J. Chem. Phys.* **1984**, *81* (4), 2047−2052.
(36) Duke, T.; Holy, T. E.; Leibler, S. *Phys. Rev. Lett.* **1995**, *74* (2), 330−333.
(37) Nitta, T.; Tanahashi, A.; Obara, Y.; Hirano, M.; Razumova, M.; Regnier, M.; Hess, H. *Nano Lett.* **2008**, *8* (8), 2305−2309.
(38) Nitta, T.; Tanahashi, A.; Hirano, M. *Lab Chip* **2010**, *10* (11), 1447−1453.
(39) Hess, H.; Clemmens, J.; Qin, D.; Howard, J.; Vogel, V. *Nano Lett.* **2001**, *1* (5), 235−239.
(40) Vikhorev, P. G.; Vikhoreva, N. N.; Sundberg, M.; Balaz, M.; Albet-Torres, N.; Bunk, R.; Kvennefors, A.; Liljesson, K.; Nicholls, I. A.; Nilsson, L.; Omling, P.; Tagerud, S.; Montelius, L.; Mansson, A. *Langmuir* **2008**, *24* (23), 13509−13517.
(41) Serrano, C. G.; McDermott, J. J.; Velegol, D. *Nat. Mater.* **2011**, *10* (9), 716−721.
(42) Brinker, C. J.; Lu, Y. F.; Sellinger, A.; Fan, H. Y. *Adv. Mater.* **1999**, *11* (7), 579−585.
(43) Hong, Y.; Blackman, N. M. K.; Kopp, N. D.; Sen, A.; Velegol, D. *Phys. Rev. Lett.* **2007**, *99* (17), 178103.
(44) Tucker, R.; Katira, P.; Hess, H. *Nano Lett.* **2008**, *8* (1), 221−226.
(45) Kay, Euan R.; Leigh, David A.; Zerbetto, F. *Angew. Chem., Int. Ed.* **2007**, *46* (1−2), 72−191.
(46) Howard, J.; Hunt, A. J.; Baek, S. *Methods Cell. Biol.* **1993**, *39*, 137−47.
(47) Coy, D. L.; Wagenbach, M.; Howard, J. *J. Biol. Chem.* **1999**, *274* (6), 3667−71.